

Discontinuous isogeometric boundary element (IGABEM) formulations in 3D automotive acoustics

Yi Sun^{a,b,c,d,*}, Jon Trevelyan^a, Gabriel Hattori^{a,e}, Chihua Lu^{b,c,d}

^a*Department of Engineering, Durham University, South Road, Durham, UK*

^b*School of Automotive Engineering, Wuhan University of Technology, Wuhan 430070, China*

^c*Hubei Key Laboratory of Advanced Technology for Automotive Components (Wuhan University of Technology), Wuhan 430070, China*

^d*Hubei Collaborative Innovation Center for Automotive Components Technology (Wuhan University of Technology), Wuhan 430070, China*

^e*Department of Engineering, University of Cambridge, CB2 1PZ, Cambridge, UK*

Abstract

The isogeometric boundary element method (IGABEM) is a technique that employs non-uniform rational B-splines (NURBS) as basis functions to discretise the solution variables as well as the problem geometry in a boundary element formulation. IGABEM has shown improved convergence properties over the conventional boundary element method (BEM) algorithms. However, in acoustics, IGABEM has only been applied to problems with simple smooth boundary conditions. In most real-world engineering design and analysis acoustic problems, geometric corners and discontinuities in boundary conditions can give rise to more complexity in the solution field that may be more efficiently modelled using a discontinuous approach.

In the current work we develop a discontinuous IGABEM formulation based on discontinuous elements and a suitable collocation scheme. Continuous and discontinuous formulations are compared. In this paper, a three dimensional model with different sets of boundary conditions is presented to explore the conditions under which a discontinuous formulation outperforms the continuous IGABEM. A simple car passenger compartment model characterised by panels

*Corresponding author

Email address: yi.sun@whut.edu.cn (Yi Sun)

with piecewise continuous impedance boundaries is presented to illustrate the potential of the proposed method for integrated engineering design and analysis.

Keywords: NURBS, discontinuous IGABEM, car passenger compartment, interior acoustic problem

1. INTRODUCTION

The noise, vibration and harshness (NVH) performance is one of the most important indicators in evaluating the quality of a vehicle. The driver's fatigue, vehicle riding comfort and the durability of components will be influenced by any interior noise and vibration [1, 2]. These factors have led vehicle engineers to develop more accurate and effective methods to reduce the noise and vibration inside the passenger compartment. The development of these methods is underpinned by advanced computational modelling. Many Computer Aided Engineering (CAE) techniques are available for acoustic analysis, among them the Finite Element Method (FEM) [3, 4] and Boundary Element Method (BEM) [5–9] are the most widely used of the deterministic methods. We note that for asymptotically high frequency problems, the methods based on optics, e.g. the ray tracing method [10, 11] and the Geometrical Theory of Diffraction [12, 13], are popular, but our focus is the lower frequency range within automobile passenger compartments. The BEM is popular with engineers for acoustic solutions because of its accuracy and the ease of considering infinite domains for problem involving radiation or scattering bodies. The BEM involves the problem discretisation and solution on the boundary of the domain [14–16], which reduces the complexity of mesh generation and the size of the problem.

Although these tools have led to shorter design cycles, their practical application still involves some complications in producing an analysis-ready CAE model from NURBS-based CAD data. As a result, the geometry preparation and mesh generation remain time-consuming, especially for industrially relevant problems where mesh generation and refinement can take up to 80% of the total analysis time [17]. In the automotive industry, the gap between CAD and CAE

presents a considerable obstacle that extends the product design cycle, since many analysis runs are commonly required in an optimisation process.

The idea of Isogeometric Analysis (IGA), based on the use of non-uniform rational B-splines (NURBS) as the FEM approximation space, was first put forward by Hughes et al. [17] and has since received considerable attention. The concept is to use the splines typically employed in CAD geometry to capture the exact geometry for analysis directly. NURBS are the standard geometry representations in CAD and have been widely used in IGA [18–22]. Certain geometries that can only be approximated by polynomial functions can be represented exactly using NURBS, such as cylinders and spheres. Hence, the gap between CAD and CAE is bridged, and more accurate engineering simulations enabled on exact geometric representations. Most importantly, use of NURBS as an approximation space in both FEM and BEM has been shown to improve convergence properties over the use of classical Lagrange polynomials.

The isogeometric boundary element method (IGABEM) combines both the IGA and BEM. Thus the discretisation is based on a CAD construction instead of the piecewise polynomials used in the conventional BEM. By taking NURBS as the basis for the numerical approximation of the acoustic field, mesh generation and refinement are greatly simplified. The IGABEM has developed rapidly in recent years [23–28] and has been applied successfully to various fields, e.g. potential problems [23, 25, 29–31], elasticity [26, 32–34], electromagnetics [35, 36] and shape optimisation [37–40]. Particularly, in the area of acoustic applications, Simpson et al. [41] employed IGABEM based on T-splines to solve both interior and exterior acoustic problems. Further, Peake et al. proposed an extended isogeometric boundary element method (XIBEM) for two-dimensional Helmholtz problems in the mid-high frequency range [23] and then extended it to three dimensions [29]. It should be noted that these analyses have been performed only for smooth boundary conditions while in acoustic problems of relevance to the automobile industry, the boundary conditions are mostly discontinuous, the sound absorption properties of lining materials and windows being markedly different.

The BEM is usually presented as a mixed formulation in which one solves a system containing both the primary variable and its derivative as unknowns. For example, in elasticity problems, the primary unknown is displacement. The second unknown, traction, is related through Hooke's law to the derivative of the primary unknown. For Laplace and Helmholtz problems, the unknowns are the potential and its normal derivative. Since the normal is discontinuous across edges and at corners, one cannot use a continuous description of the derivative unknown (unless as in, for example, the acoustic probe example in [41] a homogeneous Neumann boundary is used throughout), and BEM formulations generally need to accommodate this discontinuity. The literature contains descriptions of IGABEM formulations in which the derivative unknown is expanded in a discontinuous form; for example, Scott et al. [25] and Marussig et al. [42] both study elasticity problems and use a discontinuous representation of traction. However, these authors maintain a continuous description of the primary variable, i.e. the displacement. Nevertheless, the BEM admits a fully discontinuous approach, in which both the primary unknown and its normal derivative are expressed using a discontinuous form. Thus, for example, the displacement can be discontinuous in elasticity analysis, as can be the potential in Laplace and Helmholtz problems. While discontinuity of the primary variable violates a physical constraint, a fully discontinuous discretisation can allow a more efficient numerical approximation in certain circumstances, particularly where the primary variable exhibits large gradients and/or weak discontinuities. The use of such fully discontinuous elements in conventional BEM is a mature technique, going back to some of the earliest works by Brebbia on the newly named Boundary Element Method [43] and later studied in more detail by Xu and Brebbia [44] and Parreira [45]. In this paper we apply the approach for the first time in IGABEM. This is in the context of Helmholtz problems. We mention that the discontinuous approach gives rise to additional degrees of freedom where the nodes containing the unknowns are no longer shared between elements, which will be discussed in Section 5.1. This requires more equations to be included to arrive at a square system, so a strategy for collocation point lo-

cation is required. Traditionally this is achieved by collocating internally within elements rather than at the element perimeter. We present a strategy for locating collocation points in a later section, but note that Wang and Benson [46] consider a similar problem in collocation for their nonsingular IGABEM formulation.

In this paper, comparisons are made between discontinuous IGABEM and continuous IGABEM formulations. All models are characterised by panels with piecewise continuous impedance boundaries [47–50].

The remainder of the text is structured as follows. First, an introduction to B-splines and NURBS is given in Section 2. Section 3 and Section 4 present the conventional Boundary Element Method (BEM) and implementation of IGABEM, respectively. The formulation of the discontinuous IGABEM, including the collocation scheme, is introduced in Section 5. Then, several numerical examples are given in Section 6 to verify the accuracy of the proposed scheme, including a simplified car passenger compartment subjected to realistic boundary conditions. Finally, we draw some conclusions in Section 7.

2. B-SPLINES AND NURBS

In this section we describe the mathematical preliminaries relating to B-splines and NURBS that are required as a precursor to the later sections of the paper. The interested reader is directed to [51, 52] for a full description.

2.1. B-SPLINES

The definition of B-Spline basis functions starts with the concept of the knot vector. A knot vector is constructed from a sequence of non-decreasing real numbers:

$$\Xi = \{\xi_1, \xi_2, \dots, \xi_{n+p+1}\}, \quad \xi_i \in \mathbb{R} \quad (1)$$

where ξ_i is the i -th knot in the parameter space representing the parametric coordinates of the curve, $i = 1, 2, \dots, n + p + 1$, n is the number of the basis functions which construct the B-splines, p is the curve degree. The half-open

interval $[\xi_i, \xi_{i+1})$ is called a knot span which can have zero length since the knots may be repeated. The interval $[\xi_1, \xi_{n+p+1})$ is called a patch. The B-spline basis functions can be built recursively by using the Cox-de Boor recurrence formula [53, 54] based on the knot vector:

$$p = 0 : N_{i,0}(\xi) = \begin{cases} 1 & \xi_i \leq \xi < \xi_{i+1} \\ 0 & \text{otherwise} \end{cases} \quad (2)$$

$$p > 0 : N_{i,p}(\xi) = \frac{\xi - \xi_i}{\xi_{i+p} - \xi_i} N_{i,p-1}(\xi) + \frac{\xi_{i+p+1} - \xi}{\xi_{i+p+1} - \xi_{i+1}} N_{i+1,p-1}(\xi) \quad (3)$$

B-spline curves are constructed from a linear combination of B-spline basis functions. A p -th degree piecewise polynomial B-spline curve $C^b(\xi)$ is given by

$$C^b(\xi) = \sum_{i=1}^n N_{i,p}(\xi) \mathbf{A}_i \quad (4)$$

where \mathbf{A}_i are the control points, which are position vectors determining the shape of the spline curve, and $N_{i,p}(\xi)$ denotes the i -th basis function from Eq. (3). It should be noted that the concepts of control points and basis functions are similar to nodal coordinates and shape functions in BEM, respectively, but a key difference is that control points may lie off the physical boundary.

A B-spline surface $S^b(\xi, \eta)$ is a tensor product surface of two B-splines. Given a net of control points $\mathbf{A}_{i,j}$ ($i = 1, 2, \dots, n; j = 1, 2, \dots, m$), polynomial degrees p and q , two knot vectors $\Xi = [\xi_1, \xi_2, \dots, \xi_{n+p+1}]$ and $\Theta = [\eta_1, \eta_2, \dots, \eta_{m+q+1}]$, a B-spline surface is defined as

$$S^b(\xi, \eta) = \sum_{i=1}^n \sum_{j=1}^m N_{i,p}(\xi) M_{j,q}(\eta) \mathbf{A}_{i,j} \quad (5)$$

where $N_{i,p}(\xi)$ and $M_{j,q}(\eta)$ represent univariate B-spline basis functions of degree p and q , associated with knot vectors Ξ and Θ , respectively.

2.2. KNOT REFINEMENT

In this work, h-refinement is adopted as the refinement method. In an isogeometric context this can be accomplished by knot insertion. Given a knot vector $\Lambda = \{\xi_1, \xi_2, \dots, \xi_{n+p+1}\}$, $\xi_i \in \mathbb{R}$, a knot $\bar{\xi} \in [\xi_t, \xi_{t+1}]$ can be inserted into

Λ , potentially multiple times. If $\bar{\xi}$ is to be inserted 3 times, for example, the
 130 new knot vector will be $= \{\xi_1, \xi_2, \dots, \xi_t, \bar{\xi}, \bar{\xi}, \bar{\xi}, \xi_{t+1}, \dots, \xi_{n+p+1}\}$. Associated with
 this is a change in the control points, the original set $\{Q_1, Q_2, \dots, Q_n\}$ being
 expanded and changed to $\{\bar{Q}_1, \bar{Q}_2, \dots, \bar{Q}_{n+3}\}$ through the following procedure:

$$\bar{Q}_i = \alpha_i Q_i + (1 - \alpha_i) Q_{i-1}, \quad (6)$$

where

$$\alpha_i = \begin{cases} 1, & 1 \leq i \leq t - p \\ \frac{\bar{\xi} - \xi_i}{\xi_{i+p} - \xi_i}, & t - p + 1 \leq i \leq t \\ 0, & t + 1 \leq i \leq n + p + 2 \end{cases} \quad (7)$$

It should be noted that knot insertion just changes the vector space basis as
 135 well as the basis functions, while the geometry is not changed.

2.3. NURBS

NURBS are developed from B-splines but the introduction of weights gives
 more flexibility and enables the exact representation of geometric entities like
 circular arcs and spheres [51]. By defining a positive weight ω_i to each basis
 140 function, the NURBS basis functions $R_{i,p}(\xi)$ can be expressed as

$$R_{i,p}(\xi) = \frac{N_{i,p}(\xi)w_i}{W(\xi)} \quad (8)$$

with

$$W(\xi) = \sum_{j=1}^n N_{j,p}(\xi)w_j \quad (9)$$

If all the weights are equal to 1, then $R_{i,p}(\xi) = N_{i,p}(\xi)$, and the NURBS degen-
 erate into B-splines. A p -th degree NURBS curve is obtained by

$$C(\xi) = \sum_{i=1}^n R_{i,p}(\xi) \mathbf{A}_i \quad (10)$$

The definition of a NURBS surface $S(\xi, \eta)$ is then completely analogous to a
 145 B-spline surface, given as

$$S(\xi, \eta) = \sum_{i=1}^n \sum_{j=1}^m R_{i,j,p,q}(\xi, \eta) \mathbf{A}_{i,j} \quad (11)$$

with

$$R_{i,j,p,q}(\xi, \eta) = \frac{N_{i,p}(\xi)M_{j,q}(\eta)w_{i,j}}{\sum_{\hat{i}=1}^n \sum_{\hat{j}=1}^m N_{\hat{i},p}(\xi)M_{\hat{j},q}(\eta)w_{\hat{i},\hat{j}}} \quad (12)$$

These same NURBS basis functions are also used to represent the field variables.

It should be noted that the basis functions of NURBS have some important

150 properties:

1. Non-negativity: $R_{i,j}(\xi, \eta) \geq 0$ for all i, j, ξ and η .
2. Partition of unity: $\sum_{i=1}^n \sum_{j=1}^m R_{i,j}(\xi, \eta) = 1$ for all (ξ, η) ;
3. Local support: if (ξ, η) is outside the knot span $[\xi_i, \xi_{i+p+1}) \times [\eta_j, \eta_{j+p+1})$, $R_{i,j}(\xi, \eta) = 0$;
- 155 4. Continuity: if (ξ, η) is inside the knot span $[\xi_i, \xi_{i+p+1}) \times [\eta_j, \eta_{j+p+1})$, all partial derivatives of $R_{i,j}(\xi, \eta)$ exist. At a ξ knot (η knot) it is $p - k$ ($q - k$) times differentiable in the ξ (η) direction, where k is the multiplicity of the knot.

3. Boundary Element Method (BEM)

Time-harmonic acoustic waves within the domain $\Omega \in \mathbb{R}^3$ with boundary Γ
 160 are governed by the well-known Helmholtz equation [55]:

$$\nabla^2 \phi(\mathbf{x}) + k^2 \phi(\mathbf{x}) = 0, \quad \mathbf{x} \in \Omega \quad (13)$$

where ∇^2 is the Laplacian operator, $\phi(\mathbf{x}) \in \mathbb{C}$ is the acoustic potential at the point \mathbf{x} , λ is the wavelength, and $k = 2\pi/\lambda$ is the wave number. We assume $e^{-i\omega t}$ time dependence.

We seek the solution to (13) subject to boundary conditions that may take
 165 the following forms in acoustic problems:

- Dirichlet condition: the acoustic potential is known over the boundary:

$$\phi(\mathbf{x}) = \bar{\phi}(\mathbf{x}), \quad \mathbf{x} \in \Gamma \quad (14)$$

- Neumann condition: the derivative of the acoustic potential is known over the boundary:

$$\frac{\partial\phi(\mathbf{x})}{\partial n} = \bar{q}, \quad \mathbf{x} \in \Gamma \quad (15)$$

- Robin condition: the derivative of the potential is presented as a linear function of the potential:

$$\alpha \frac{\partial\phi(\mathbf{x})}{\partial n} = \beta\phi(\mathbf{x}) + \gamma, \quad \mathbf{x} \in \Gamma \quad (16)$$

Particularly, in the context of an acoustic problem with absorbing boundaries it is often desirable to express the Robin condition in the form

$$\frac{\partial\phi(x)}{\partial n} = -i\rho_0\omega \frac{\phi(x)}{Z} \quad (17)$$

where ρ_0 is the material density, ω is the frequency and Z is the boundary impedance, given by the acoustic pressure divided by the velocity of the fluid relative to that of the structure [56]. We note the frequency dependence of the impedance properties.

Using standard techniques, Eq. (13) can be reformulated as a boundary integral equation (BIE):

$$C(\mathbf{s}) + \int_{\Gamma} \frac{\partial G(\mathbf{s}, \mathbf{x})}{\partial n} \phi(\mathbf{x}) d\Gamma(\mathbf{x}) = \int_{\Gamma} G(\mathbf{s}, \mathbf{x}) \frac{\partial\phi(\mathbf{x})}{\partial n} d\Gamma(\mathbf{x}) \quad (18)$$

where $\mathbf{s} \in \Gamma$ represents the source point, n is the unit outward pointing normal, $C(\mathbf{s})$ is a jump-term depending on the geometry at the source point. If the source point lies on a smooth surface, the jump term $C(\mathbf{s})=1/2$. $\phi(\mathbf{x})$ and $\frac{\partial\phi(\mathbf{x})}{\partial n}$ are the acoustic potential and its derivative, respectively.

By substituting Eq. (17) into Eq. (18), the BIE with the impedance boundary condition applied can be obtained as follows:

$$C(\mathbf{s}) + \int_{\Gamma} \left(\frac{\partial G(\mathbf{s}, \mathbf{x})}{\partial n} + i\rho_0\omega \frac{G(\mathbf{s}, \mathbf{x})}{Z} \right) \phi(\mathbf{x}) d\Gamma(\mathbf{x}) = 0 \quad (19)$$

This will guide the following work of the acoustic problem of a passenger compartment in Section 6.2.

For 3D problems, $G(\mathbf{s}, \mathbf{x})$ is the Green's function given by:

$$G(\mathbf{s}, \mathbf{x}) = \frac{e^{ikr}}{4\pi r} \quad (20)$$

$\partial G(\mathbf{s}, \mathbf{x})/\partial n$ is the corresponding derivative expressed as:

$$\frac{\partial G(\mathbf{s}, \mathbf{x})}{\partial n} = \frac{e^{ikr}}{4\pi r^2} (ikr - 1) \frac{\partial r}{\partial n} \quad (21)$$

and

$$r = |\mathbf{x} - \mathbf{s}| \quad (22)$$

190 The integrals in Eq. (18) contain a weak singularity and any of the standard techniques in the BEM literature may be used to evaluate them [57–59].

In the conventional BEM, the boundary Γ is discretised into E non-overlapping boundary elements, which can be expressed as:

$$\Gamma = \bigcup_{e=1}^E \Gamma_e \quad (23)$$

195 The elements represent the geometry through the mapping:

$$\Gamma_e = \mathbf{F}_e(\bar{\xi}, \bar{\eta}), \quad \bar{\xi}, \bar{\eta} \in [-1, 1] \quad (24)$$

then Eq. (19) can be written as a discretised form:

$$C(\mathbf{s}) + \sum_{e=1}^E \sum_{m=1}^M P_{em}(\mathbf{s}) \phi_{em} = \sum_{e=1}^E \sum_{m=1}^M Q_{em}(\mathbf{s}) \frac{\partial \phi_{em}}{\partial n} \quad (25)$$

where

$$P_{em} = \int_{-1}^1 \int_{-1}^1 \frac{\partial G(\bar{\xi}, \bar{\eta})}{\partial n} N_{em}(\bar{\xi}, \bar{\eta}) J_e(\bar{\xi}, \bar{\eta}) d\bar{\xi} d\bar{\eta} \quad (26)$$

$$Q_{em} = \int_{-1}^1 \int_{-1}^1 G(\bar{\xi}, \bar{\eta}) N_{em}(\bar{\xi}, \bar{\eta}) J_e(\bar{\xi}, \bar{\eta}) d\bar{\xi} d\bar{\eta} \quad (27)$$

where M is the number of nodes on the element, N_{em} are the corresponding shape functions, and J_e is the Jacobian from the mapping in Eq. (24).

200 Taking the point \mathbf{s} to lie at each node in turn, the collocation form of the BIE yields a set of equations relating all potential and velocity coefficients as follows:

$$\mathbf{H}\mathbf{u} = \mathbf{G}\mathbf{q} \quad (28)$$

where \mathbf{u} , \mathbf{q} are vectors containing nodal values of ϕ , $\frac{\partial \phi}{\partial n}$. The fully populated matrix \mathbf{H} contains all integrals of the left-hand side terms of Eq. (25), and

matrix \mathbf{G} is assembled by integrals of the right-hand side terms of Eq. (25).
 205 ϕ and $\partial\phi/\partial n$ are vectors containing acoustic potential and normal derivative coefficients, respectively.

By reordering all the unknowns and related coefficients to the left-hand side and all the knowns and related coefficients to the right-hand side, we obtain a linear system:

$$\mathbf{Ax} = \mathbf{b} \quad (29)$$

210 where \mathbf{A} is an unsymmetrical and fully populated square matrix, the vector \mathbf{x} contains all unknown potential and derivative coefficients while the vector \mathbf{b} is calculated from all known coefficient and their associated terms. Eq. (29) is a linear system which can be solved directly.

The BIE can be applied to both bounded and unbounded (infinite) domains.
 215 However, for the case of unbounded domains, it is well known to result in a singular system at wave numbers corresponding to the eigenfrequencies of the interior problem formed on the boundary Γ . The present work is entirely aimed at bounded domains modelling automotive passenger compartments, so there is no consideration of the strategies (CHIEF[60], Burton-Miller[61]) that are
 220 widely used to overcome this system degeneracy.

4. IGABEM for Acoustics

Instead of polynomial shape functions, NURBS basis functions are employed to represent ϕ , $\partial\phi/\partial n$ as well as the geometry in the IGABEM. The boundary is divided into E non-overlapping isogeometric patches Γ_e , analogously to the
 225 conventional BEM in Eq. (23). A local coordinate mapping is defined on each patch Γ_e as follows:

$$\Gamma_e = \mathbf{F}_e(u, v), \quad u, v \in [0, 1] \quad (30)$$

It should be noted that the integration is calculated knot span by knot span, e.g. $[\xi_i, \xi_{i+1}] \times [\eta_j, \eta_{j+1}]$ (see Figure 1(a)), while in the integration using Gauss-Legendre quadrature, the parametric system $Y = (\bar{\xi}, \bar{\eta})$ is defined in $[-1, 1] \times$
 230 $[-1, 1]$. Figure 1 shows the coordinate transformation in the IGABEM. This

requires that an additional transformation be defined to map from the local coordinates to the parametric space.

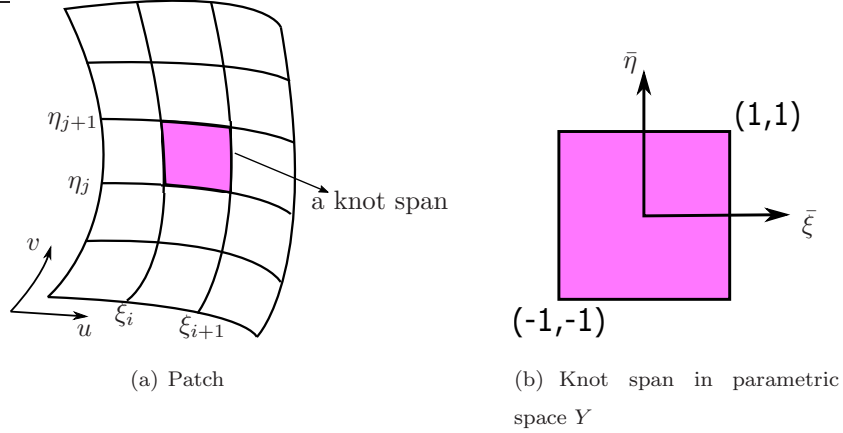


Figure 1: Coordinate transformation in IGABEM.

The total Jacobian can be expressed as:

$$J_Y = \left| \frac{\partial \mathbf{x}}{\partial \mathbf{F}} \frac{\partial \mathbf{F}}{\partial \mathbf{Y}} \right| \quad (31)$$

where the first component is the Jacobian mapping from the global to local coordinates on each patch, and the second term is the Jacobian mapping from local coordinates to the parametric space.

The acoustic potential and the normal derivative can be discretised in terms of a NURBS expansion, respectively:

$$\phi(\mathbf{x}) = \sum_{i=1}^n \sum_{j=1}^m R_{i,j,p,q}(u(\mathbf{x}), v(\mathbf{x})) \tilde{\phi}_{j,p} \quad (32)$$

$$\frac{\partial \phi(\mathbf{x})}{\partial n} = \sum_{i=1}^n \sum_{j=1}^m R_{i,j,p,q}(u(\mathbf{x}), v(\mathbf{x})) \tilde{q}_{j,p} \quad (33)$$

where n and m are the number of control points, p and q are the curve degrees in the u and v direction, respectively. $\tilde{\phi}_{j,p}$ and $\tilde{q}_{j,p}$ are the coefficients for potentials and derivatives associated with the control points. It is important to note that $\tilde{\phi}_{j,p}$ and $\tilde{q}_{j,p}$ are no longer the nodal potentials and derivatives,

but are simply coefficients from which these quantities can be recovered using
 245 (32) and (33); indeed, since the control points may not lie on the geometry it
 would be meaningless to assign a potential or potential derivative to them. The
 final isogeometric boundary integral equation can be written by substituting
 Eq. (32) and Eq. (33) into Eq. (25):

$$C(\mathbf{s}) + \sum_{e=1}^E \sum_{i=1}^n \sum_{j=1}^m P_{eij}(\mathbf{s}) \phi_{eij} = \sum_{e=1}^E \sum_{i=1}^n \sum_{j=1}^m Q_{eij}(\mathbf{s}) \frac{\partial \phi_{eij}}{\partial n} \quad (34)$$

with

$$P_{eij} = \int_{-1}^1 \int_{-1}^1 \frac{\partial G(\bar{\xi}, \bar{\eta})}{\partial n} R_{eij}(\bar{\xi}, \bar{\eta}) J_{Y_{eij}}(\bar{\xi}, \bar{\eta}) d\bar{\xi} d\bar{\eta} \quad (35)$$

$$Q_{eij} = \int_{-1}^1 \int_{-1}^1 G(\bar{\xi}, \bar{\eta}) R_{eij}(\bar{\xi}, \bar{\eta}) J_{Y_{eij}}(\bar{\xi}, \bar{\eta}) d\bar{\xi} d\bar{\eta} \quad (36)$$

where R_{eij} are the corresponding NURBS basis functions, and $J_{Y_{eij}}$ is the Ja-
 250 cobian from the mapping in Eq. (31). Here two indices i, j are used to refer to
 the control points and associated basis functions in an element, as a B-spline
 surface is obtained by taking a bidirectional net of control points, requiring two
 knot vectors such as (5).

In general, the control points are no longer able to be taken as the collocation
 255 points in IGABEM, since they may not lie on the geometry boundary (except
 in flat patches). Alternatively, the Greville abscissae [62, 63] may be used to
 define the position of collocation points in the parameter space as:

$$\xi'_g = \frac{\xi_{g+1} + \xi_{g+2} + \dots + \xi_{g+p}}{p}, \quad g = 1, 2, \dots, N \quad (37)$$

where N denotes the number of control points, and p is the degree of the
 NURBS.

260 After defining the collocation points, the boundary integral equations defined
 in Eq. (34) can be assembled in matrix form analogously to conventional BEM.

5. Discontinuous Isogeometric Boundary Element Method

5.1. Discontinuous Isogeometric Boundary Patch

Discontinuous elements have been used in conventional BEM for many years,
 265 with the nodes located away from the element edges. This allows for greater

flexibility in mesh grading, and also lends itself to parallel implementations since every term in the influence matrices H and G has only a single contribution from a single integral over an element. Here we make use of a discontinuous formulation to improve accuracy in the presence of discontinuous boundary conditions. In IGABEM, we are constrained by the definition of NURBS to have control points on the edges of the patch, requiring some adaptation in the way discontinuous elements are implemented. In order to obtain a square system (Eq. (29)), the number of collocation points must be equal to the number of unknowns. In a discontinuous model, there are multiple control points in the same location, each having membership of a different patch. This evokes the idea of double nodes in early BEM literature. In order to ensure a suitable number of collocation points, the simplest scheme is to locate them internally in each patch as shown in Figure 2. The discontinuous IGABEM patches allow the potential fields to become discontinuous at the interfaces between patches. Although the true solution will have a continuous potential field, the discontinuity in boundary conditions can give rise to large potential derivatives that may be more efficiently approximated if both the potential and derivative are approximated in a discontinuous basis.

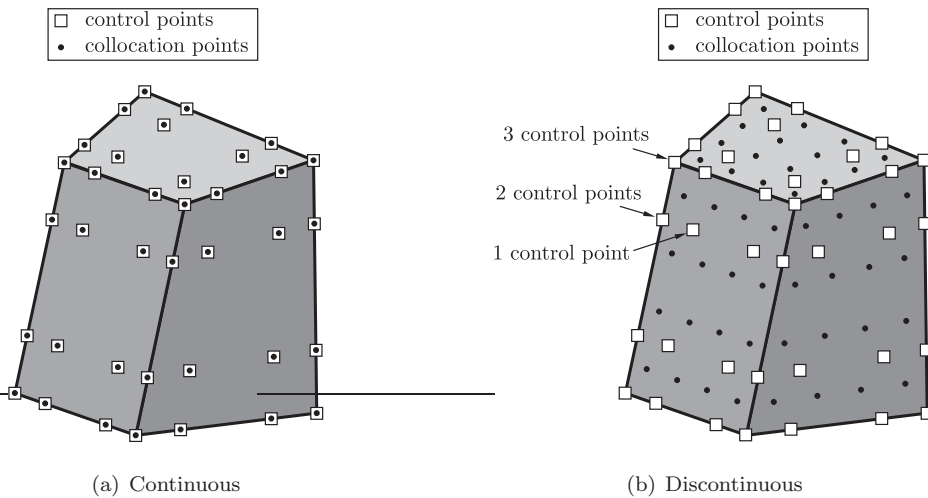


Figure 2: Isogeometric patches in 3D.

5.2. Collocation

285 With discontinuous elements, a collocation strategy is needed because some control points will be coincident, but collocation at coincident points will lead to identical equations giving a rank-deficient system. In the IGABEM schemes introduced in the current work, collocation points are separated from the control points that are associated with the concept of a node in the conventional BEM. 290 Marburg [64] studied a long duct and a vehicle cabin to investigate the location of nodal points in discontinuous Lagrangian boundary elements, and found for low-order elements that discontinuous elements gave smaller errors than continuous ones if the nodal points were located at the zeroes of the Legendre polynomials. It should be noted that this was observed only for a pure Neumann 295 problem. Additionally, it was observed that the optimal locations of collocation points were different when the frequency changed, which is likely to be due to the boundary conditions. In this paper, we make a preliminary study of collocation point locations for discontinuous elements in the IGABEM framework. We make no attempt to determine a mathematically optimal distribution, but 300 compare three candidate collocation schemes, as follows, to determine a suitable scheme to take forward in the remainder of this paper:

1. *Uniform collocation*: where the collocation points are uniformly distributed in the parameter domain.
2. *Legendre polynomials*: where the collocation points are generated at the 305 roots of Legendre polynomials in the parameter domain.
3. *Modified-Greville abscissae*: where the parameters correspond to collocation points defined by a Modified-Greville abscissae definition studied in [46], moving the first and the last collocation points away from the edges of the patches. Initially, the collocation points are generated as the Greville 310 abscissae along each direction in the parameter space as

$$\xi_i' = \frac{1}{p}(\xi_{i+1} + \xi_{i+2} + \dots + \xi_{i+p}) \quad i = 1, 2, \dots, N, \quad (38)$$

where p is the degree of the NURBS, and N is the number of control points in the ξ direction.

Then, a coefficient β is brought in to move the first and the last collocation points of Eq. (38) inside the patch as

$$\xi'_1 = \xi'_1 + \beta(\xi'_2 - \xi'_1) \quad (39)$$

$$\xi'_n = \xi'_n + \beta(\xi'_n - \xi'_{n-1}) \quad (40)$$

where the coefficient $\beta = 0.5$ has been proved to be the optimal value [46].

Figure 3 shows the different locations of collocation points in parametric space according to the three schemes. In this case, in both parametric directions we have knot vector $\Upsilon = \{0, 0, 0, 1, 1, 1\}$, $p = 2$ and $N = 3$.

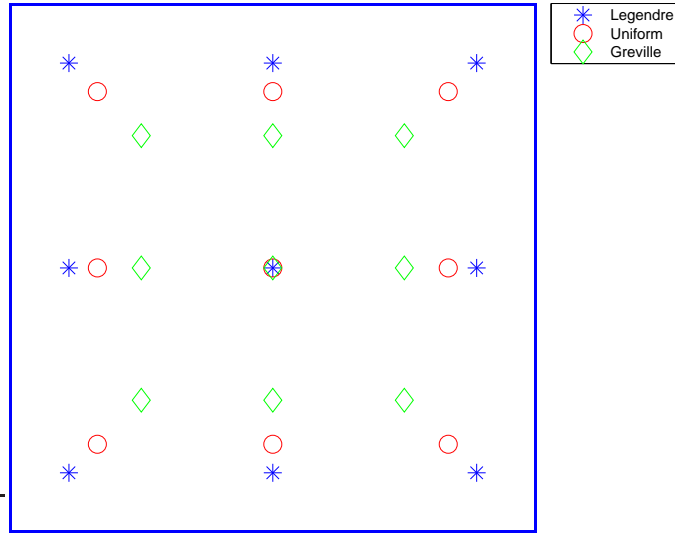


Figure 3: Collocation methods in parametric domain.

It should be noticed that DOF that are normally shared between adjacent elements are no longer shared so that the total number of DOF increases compared to a continuous element model having the same number of elements. This can mean that a smaller number of elements is required to achieve the same accuracy, so it is not obvious whether a continuous or discontinuous approach is

preferred. In this work, the comparison between the different collocation methods is based on meshes with the same number of DOF instead of with the same number of elements.

325 We study the convergence for a simple problem using the three collocation schemes to decide which strategy to use in this work. First we consider the acoustic field inside a cubic cavity lying in $(x, y, z) \in [0, 3]^3$, with dimensions in metres. We analyse the case of a plane wave, of wavelength $\lambda = 5$ m, propagating through the cube in the x -direction. This is a rather low frequency
 330 case, a choice driven by the conditions in the application example we focus on in automotive engineering.

The Dirichlet boundary condition $\bar{\phi} = 1$ is applied on the patch lying in $x = 0$, and the Neumann condition with

$$\bar{q} = -k \sin 3k + ik \cos 3k \quad (41)$$

is applied on the patch lying in $x = 3$, as it is the analytical solution of the
 335 derivative on the corresponding patch. A Neumann condition with $\bar{q} = 0$ is applied on all other patches.

The L_2 norm of the potential was calculated over the entire boundary as:

$$\|\phi\|_{L_2(\Gamma)} = \sqrt{\int_{\Gamma} |\phi|^2 d\Gamma} \quad (42)$$

We define an error metric ϵ evaluated as

$$\epsilon = \frac{\|\phi - \phi_{ref}\|_{L_2(\Gamma)}}{\|\phi_{ref}\|_{L_2(\Gamma)}} \quad (43)$$

where ϕ_{ref} is the reference solution obtained from the converged result of a
 340 conventional BEM analysis using quadratic shape functions.

Figure 4 shows the convergence of the error norm ϵ with respect to the number of the degree of freedom, N_d , and suggests that, in the case of quadratic uniform knot vectors, uniformly distributed collocation points give rise to faster convergence and provide a more accurate result compared to the other two
 345 strategies.

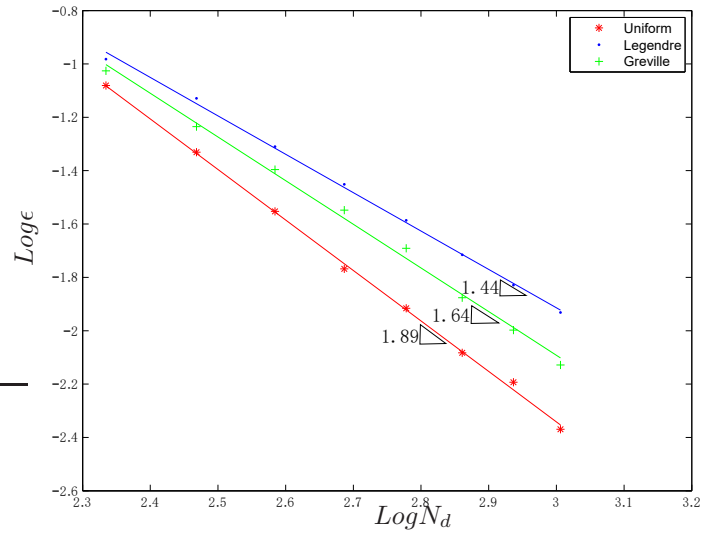


Figure 4: Comparison between collocation methods based on a cube model.

Another example using the geometry of a quarter cylinder is analysed to reinforce the conclusion drawn above. The cylinder geometry is shown in Figure 5. The rear surface of the cylinder lies in $z = 0$ while the forward facing surface lies in $z = 3$ of the Cartesian space, with dimensions in metres. We consider a spherical wave of wavelength $\lambda = 5 \text{ m}$, emanating from a point source located at $[0, 0, 6]$, passing through the domain.

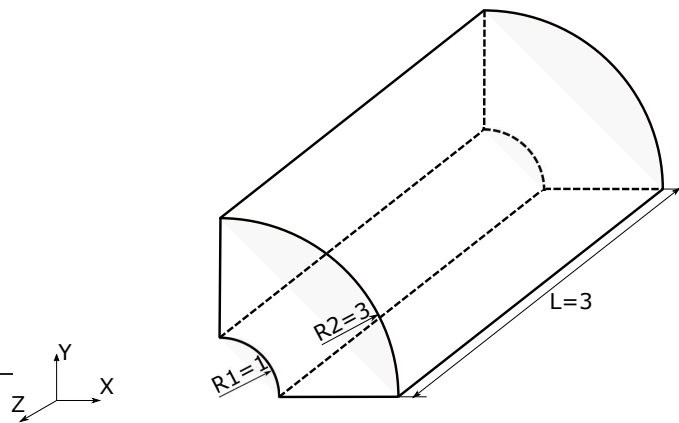


Figure 5: A quarter cylinder.

The Neumann condition with

$$\bar{q} = 3(ikr - 1)e^{ikr} / 2\pi r^3 \quad (44)$$

is applied on the patch lying in $z = 0$, and a Neumann condition with

$$\bar{q} = 3(1 - ikr)e^{ikr} / 4\pi r^3 \quad (45)$$

is applied on the patch lying in $z = 3$, where r is the distance from the source
 355 points. In addition, the Dirichlet boundary condition $\bar{\phi} = e^{ikr} / 4\pi r$ is applied
 on all remaining patches. Figure 6 shows the calculation result of this problem,
 from which we can also see that the uniform collocation method gives rise to
 faster convergence and higher accuracy compared to the other two collocation
 strategies. This agrees with the conclusion we draw from the cube problem.
 360 Thus from the two sets of results we proceed to the remaining analyses using
 uniformly distributed collocation points.

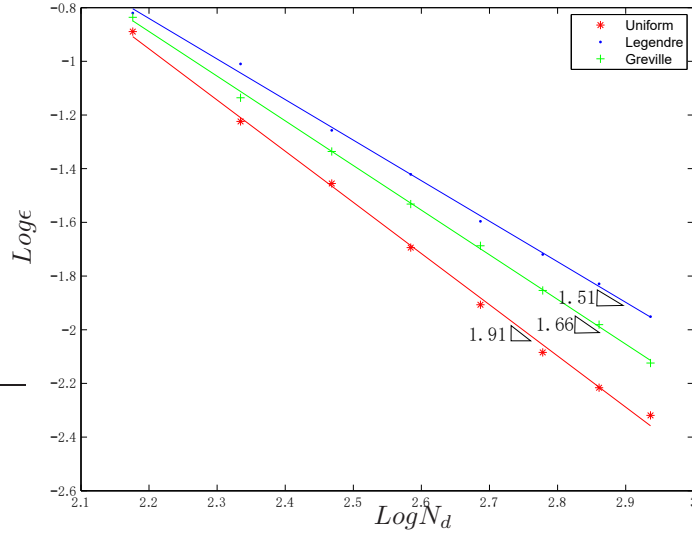


Figure 6: Comparison between collocation methods based on a quarter cylinder model.

6. NUMERICAL EXAMPLES

6.1. Cube

This section presents a numerical example to investigate the accuracy of the
365 proposed discontinuous IGABEM and evaluate the performance between the
IGABEM and BEM, considering both continuous and discontinuous approaches.
The problem is depicted in Figure 7. The cubic domain is constructed by 10
piecewise continuous impedance patches on which different boundary conditions
are applied. The cubic cavity lies in $(x, y, z) \in [0, 3]^3$, with dimensions in metres.
370 We define patch 1 as the small square patch $\{(y, z) \in [1, 2]^2, x = 3\}$ and patch 2
as the patch lying in the plane $x = 0$. The wavelength is $\lambda = 5 m$ in this case.

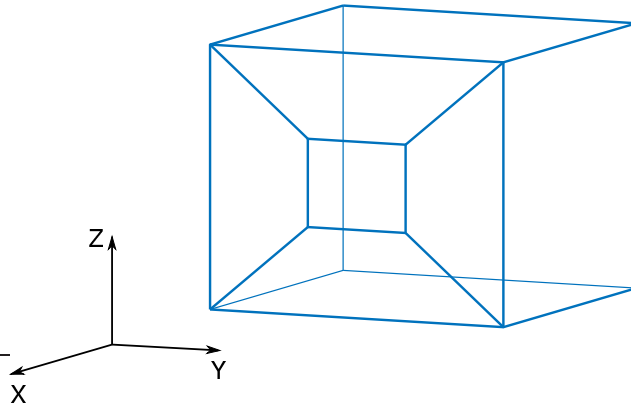


Figure 7: A 3D cubic model with piecewise continuous impedance boundaries.

In this example, two sets of boundary conditions are applied. These are
chosen to give the problem the character of a glass panel surrounded by an
absorbing material.

375 (1) A Neumann condition with $\bar{q} = 0$, $\bar{q} = 1$ is applied on patch 1 and patch
2, respectively, and a Robin condition with $\alpha = 1$, $\beta = -2$, $\gamma = 1 + i$ is applied
on the remaining patches.

Figure 8 shows the comparison for the accuracy and convergence between the
proposed method and the discontinuous BEM as well as a comparison between
380 continuous BEM and IGABEM; it is clear that IGABEM offers a significant

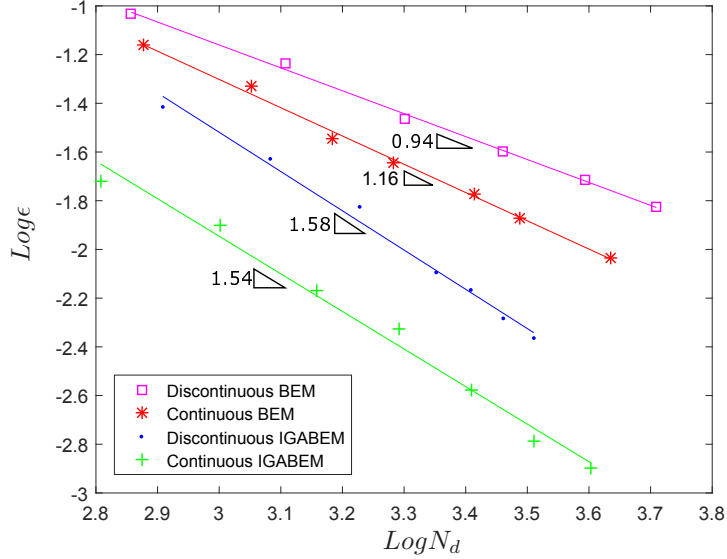


Figure 8: Comparison between BEM and IGABEM (continuous and discontinuous) for first set of boundary conditions.

advantage over BEM in accuracy for any given problem size. Also, the discontinuous IGABEM converges faster than discontinuous BEM. However, discontinuous IGABEM did not show any improvement compared to continuous IGABEM for this set of boundary conditions.

385 (2) A Neumann condition with $\bar{q} = 0$, $\bar{q} = 1$ is applied on patch 1 and patch 2, respectively. A Robin condition with $\alpha = 1$, $\beta = 10$, $\gamma = 1 + i$ is applied on the rest of the patches. The results are evaluated in the same way as in the previous example. Figure 9 shows the error comparison between different methods, and this shows contrary behaviour from the first set of boundary condition. In this
 390 example, the discontinuous IGABEM outperforms the continuous IGABEM.

It is clear that the two sets of boundary conditions give two different results for continuous and discontinuous IGABEM. Next we study different sets of boundary conditions also based on the cube model to determine the conditions for the discontinuous IGABEM outperforming the continuous IGABEM.
 395 All the boundary conditions are fixed except for the value of $\left| \frac{\beta}{\alpha} \right|$, which we vary

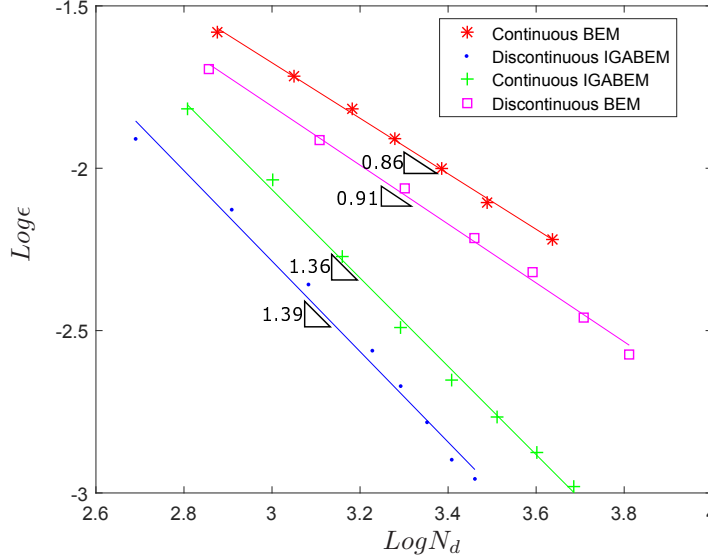


Figure 9: Comparison between BEM and IGABEM (continuous and discontinuous) for the second set of boundary conditions.

from 1 to 20. Table 1 shows the comparison between conventional IGABEM and discontinuous IGABEM using the error as defined in Eq. (42), where C denotes the continuous IGABEM, D denotes the discontinuous IGABEM, ‘coarse’ describes a model in which 4×4 control points are used on each patch, while
400 ‘refined’ means that 12×12 control points are used. The last column of the Table represents the recommendation for continuous or discontinuous depending on the value of $\left| \frac{\beta}{\alpha} \right|$. One can conclude that the discontinuous IGABEM outperforms the continuous IGABEM when the value of $\left| \frac{\beta}{\alpha} \right|$ is greater than 5.

6.2. Simplified vehicle model

405 In this section, a simplified interior acoustic problem of a vehicle passenger compartment is presented. The acoustic potential at a certain interior point is studied based on several sets of boundary conditions.

The interior sound field can be simulated in the acoustic cavity subject to three different boundary conditions:

Table 1: A set of Robin boundary conditions studied.

$ \beta/\alpha $	Error				C or D
	C coarse	C refined	D coarse	D refined	
1	0.0359	0.0053	0.0681	0.0152	C
2	0.0361	0.0051	0.0672	0.0149	C
3	0.0378	0.0052	0.0641	0.0125	C
4	0.0382	0.0042	0.0585	0.0085	C
5	0.0397	0.0051	0.0394	0.0048	D
6	0.0428	0.0051	0.0322	0.0039	D
7	0.0424	0.0052	0.0342	0.0036	D
8	0.0435	0.0055	0.0328	0.0032	D
9	0.0452	0.0056	0.0319	0.0033	D
10	0.0398	0.0056	0.0263	0.0039	D
15	0.0465	0.0053	0.0306	0.0037	D
20	0.0452	0.0061	0.0291	0.0031	D

410

(1) If a boundary surface is oscillating, e.g. the vehicle dashboard, the boundary condition can be expressed in a Neumann condition form:

$$\frac{\partial\phi(\mathbf{x})}{\partial n} = -i\rho_0\omega v \quad (46)$$

where $\rho_0 = 1.29 \text{ kg/m}^3$ is the air density, $\omega = 2\pi C/\lambda$ is the circular frequency of the acoustic source, $C = 340.29 \text{ m/s}$ is the sound speed, $\lambda = 5 \text{ m}$ is the wave length and v is the amplitude of the normal component of the velocity on the surface. In this study we take v to be 1.452 mm/s following Zhu [65].

(2) If the boundary surface is fully reflective, e.g. the window glass, the boundary condition on the surface can be expressed as a homogeneous Neumann condition form:

$$\frac{\partial\phi(\mathbf{x})}{\partial n} = 0 \quad (47)$$

(3) For absorbing boundaries, e.g. the interior lining material for the automobile, the boundary condition can be expressed as a Robin condition form:

$$\frac{\partial \phi(\mathbf{x})}{\partial n} = -i\rho_0\omega \frac{\phi(\mathbf{x})}{Z} \quad (48)$$

425 taking $\rho_0 = 1.29 \text{ kg/m}^3$ as the air density, frequency $\omega = 712 \text{ rad/s}$ and wavelength $\lambda = 3 \text{ m}$. We follow the approach of Marburg [56] to determine the acoustic impedance; here, an average admittance Y_z was obtained experimentally as

$$Y_z = \frac{f}{2800} \quad (49)$$

where f denotes the frequency in Hz. The impedance, Z , is the reciprocal of Y_z .

430 In the current work we are considering the acoustics of a vehicle compartment at a frequency of 113 Hz. The BIE with the impedance boundary condition applied can be found in Eq. (19).

The passenger compartment model is characterised by 22 piecewise continuous impedance patches as shown in Fig. 10. The sub-wavelength details of the 435 compartment are omitted as they do not contribute significantly to the solution. The first Neumann boundary condition is applied on the blue panels as they represent the vehicle dashboard. The second Neumann boundary condition is applied on the grey panels as they represent the windows of the vehicle. A Robin condition is applied on the remaining panels which represent the vehicle 440 inner lining materials.

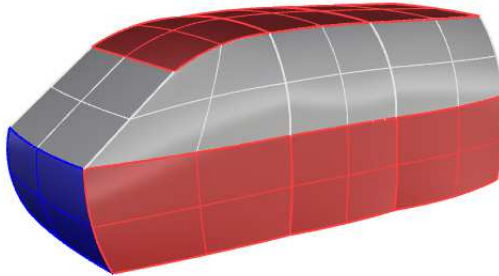


Figure 10: A simplified car model.

In this example, the converged result of a conventional BEM analysis using quadratic shape functions is taken as the reference solution. Figure 11 presents the result comparison between the three different BEM schemes, from which we can conclude that discontinuous IGABEM outperforms the conventional BEM and continuous IGABEM in this approximation to a real vehicle problem. In this case using realistic material properties, the value of β/α in the Robin condition is 37, so that these results agree with the conclusion of the analysis in Section 6.1 that the discontinuous IGABEM can provide a more accurate result than IGABEM when $\beta/\alpha > 5$. In addition, the acoustic potential at a certain point inside the model representing the position near the driver's ear has also been studied, shown in Figure 12. This result converges faster with the discontinuous IGABEM formulation and shows that the discontinuous IGABEM scheme is a promising method for simulating passenger compartment acoustics in the automotive sector.

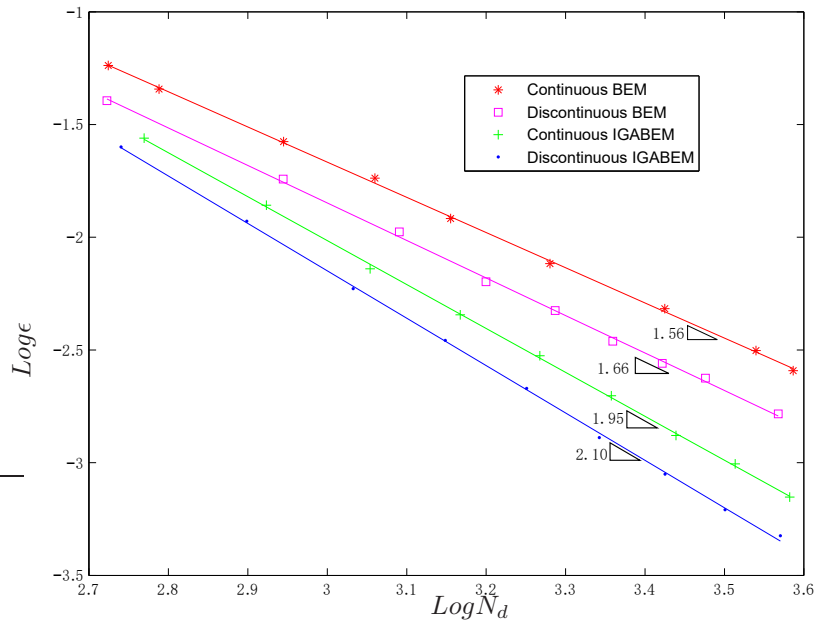


Figure 11: Comparison between BEM and IGABEM (continuous and discontinuous) of the vehicle model.

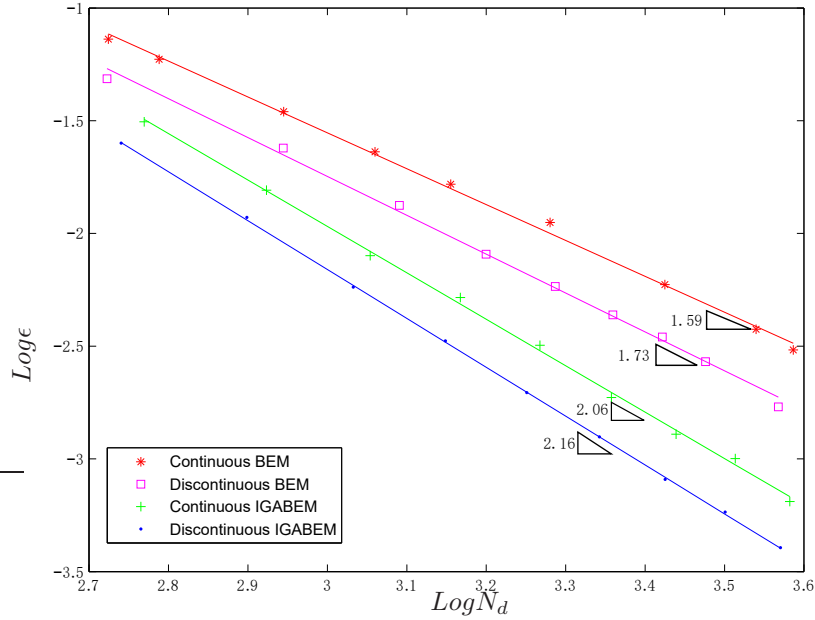


Figure 12: The interior potential near the driver's ear.

455 7. Conclusions

A fully discontinuous IGABEM for acoustic problems has been presented for the first time in this work. The discontinuous boundary patch has the ability to more efficiently approximate acoustic fields that exhibit large derivatives in the presence of discontinuous boundary conditions. The evaluation of discontinuity
460 in IGABEM modelling of 3D acoustic problems with different sets of boundary conditions has been presented and compared to the conventional IGABEM approach as well as to the conventional BEM in its continuous and discontinuous forms. It has been shown that for certain absorbing materials, the continuous IGABEM presents lower errors and converges faster than the same problem with
465 discontinuous IGABEM, while in other situations, the result is reversed. A simplified vehicle model subjected to realistic boundary conditions commonly found in automotive applications has also been presented. The result shows that in this vehicle application, the discontinuous IGABEM performs better than the continuous form. The proposed method has shown the ability to predict the

470 interior noise level in passenger compartments effectively and reduce the vehicle
design cycle, and we expect this result to have implications on software methods
used in industry in the future.

Acknowledgement

Yi Sun would like to thank the China Scholarship Council (CSC) and the
475 111 project (B17034) for the support provided to this research.

- [1] L. Morello, L. R. Rossini, G. Pia, A. Tonoli, *Noise, Vibration, Harshness*, Springer Netherlands, Dordrecht, 2011, pp. 239–363.
- [2] K. Hussain, K. Peat, Boundary element analysis of low frequency cavity acoustical problems, *Journal of Sound and Vibration* 169 (1994) 197 – 209.
- 480 [3] L. L. Thompson, A review of finite-element methods for time-harmonic acoustics, *The Journal of the Acoustical Society of America* 119 (2006) 1315–1330.
- [4] O. Zienkiewicz, R. Taylor, *The Finite Element Method—The Three Volume Set*, 6th ed., Butterworth-Heinemann ed., 2005.
- 485 [5] C. A. Brebbia, R. D. Ciskowski, *Boundary Element Methods in Acoustics*, Computational Mechanics Publications (1991).
- [6] J. He, X. Jin, Q. Zhang, Powertrain mount system optimization based on interior noise analysis, *2010 2nd International Conference on Future Computer and Communication* 24 (2010) 118–173.
- 490 [7] L. Franzoni, J. Rouse, T. Duvall, A broadband energy-based boundary element method for predicting vehicle interior noise, *The Journal of the Acoustical Society of America* 115(5) (2004) 2538–2538.
- [8] P. Banerjee, R. Butterfield, *Boundary Element Methods in Engineering Science*, McGraw-Hill (1981).

- 495 [9] T. Wu, *Boundary Element Acoustics: Fundamentals and Computer Codes*, WIT Press (2000).
- [10] A. Krokstad, S. Strom, S. Sørdsal, Calculating the acoustical room response by the use of a ray tracing technique, *Journal of Sound and Vibration* 8 (1968) 118 – 125.
- 500 [11] A. Le Bot, A. Bocquillet, Comparison of an integral equation on energy and the ray-tracing technique in room acoustics, *The Journal of the Acoustical Society of America* 108 (2000) 1732–1740.
- [12] J. B. Keller, Geometrical theory of diffraction, *Journal of the Optical Society of America* 52 (1962) 116–130.
- 505 [13] N. Tsingos, T. Funkhouser, A. Ngan, I. Carlbom, Modeling acoustics in virtual environments using the uniform theory of diffraction, in: *Proceedings of the 28th Annual Conference on Computer Graphics and Interactive Techniques, SIGGRAPH '01*, ACM, New York, NY, USA, 2001, pp. 545–552.
- 510 [14] S. Kirkup, *The Boundary Element Method in Acoustics*, Hebden Bridge: integrated sound software ed., 1998.
- [15] L. C. Wrobel, M. H. Aliabadi, *The Boundary element method*, Chichester : Wiley, 2002.
- [16] A. A. Becker, *The boundary element method in engineering : a complete course.*, London ; New York : McGraw-Hill, 1992.
- 515 [17] T. J. R. Hughes, J. Cottrell, Y. Bazilevs, Isogeometric analysis: CAD, finite elements, NURBS, exact geometry and mesh refinement, *Computer Methods in Applied Mechanics and Engineering* 194 (2005) 4135–4195.
- [18] L. Coox, E. Deckers, D. Vandepitte, W. Desmet, A performance study of NURBS-based isogeometric analysis for interior two-dimensional time-harmonic acoustics, *Computer Methods in Applied Mechanics and Engineering* 305 (2016) 441 – 467.
- 520

- [19] T. J. R. Hughes, J. A. Evans, A. Reali, Finite element and NURBS approximations of eigenvalue, boundary-value, and initial-value problems, *Computer Methods in Applied Mechanics and Engineering* 272 (2014) 290 – 320.
- [20] J. A. Cottrell, T. J. R. Hughes, A. Reali, Studies of refinement and continuity in isogeometric structural analysis, *Computer Methods in Applied Mechanics and Engineering* 196 (2007) 4160 – 4183.
- [21] J. A. Cottrell, T. J. R. Hughes, Y. Bazilevs, *Isogeometric analysis: toward integration of CAD and FEA*, John Wiley and Sons, 2009.
- [22] V. P. Nguyen, C. Anitescu, S. P. A. Bordas, T. Rabczuk, *Isogeometric analysis: An overview and computer implementation aspects*, *Mathematics and Computers in Simulation* 117 (2015) 89 – 116.
- [23] M. Peake, J. Trevelyan, G. Coates, Extended isogeometric boundary element method (XIBEM) for two-dimensional Helmholtz problems, *Computer Methods in Applied Mechanics and Engineering* 259 (2013) 93–102.
- [24] K. Li, X. Qian, *Isogeometric analysis and shape optimization via boundary integral*, *Computer-Aided Design* 43(11) (2011) 1427–1437.
- [25] M. Scott, R. Simpson, J. Evans, S. P. A. Bordas, T. J. R. Hughes, T. Sederberg, *Isogeometric boundary element analysis using unstructured T-splines*, *Computer Methods in Applied Mechanics and Engineering* 254 (2013) 197–221.
- [26] R. Simpson, S. Bordas, H. Lian, J. Trevelyan, *An isogeometric boundary element method for elastostatic analysis: 2D implementation aspects*, *Computers and Structures* 118 (2013) 2–12.
- [27] K. Belibassakis, T. Gerostathis, K. Kostas, C. Politis, P. Kaklis, A. Ginnis, C. Feurer, *A BEM-isogeometric method for the ship wave-resistance problem*, *Ocean Engineering* 60 (2013) 53 – 67.

- 550 [28] S. Li, J. Trevelyan, W. Zhang, D. Wang, Accelerating isogeometric boundary element analysis for 3-dimensional elastostatics problems through black-box fast multipole method with proper generalized decomposition, *International Journal for Numerical Methods in Engineering* 114 (2018) 975–998.
- 555 [29] M. Peake, J. Trevelyan, G. Coates, Extended isogeometric boundary element method (XIBEM) for three-dimensional medium-wave acoustic scattering problems, *Computer Methods in Applied Mechanics and Engineering* 284 (2015) 762–780.
- [30] Y. P. Gong, C. Y. Dong, X. C. Qin, An isogeometric boundary element method for three dimensional potential problems, *Journal of Computational and Applied Mathematics* 313 (2017) 454 – 468.
- 560 [31] S. Keuchel, N. C. Hagelstein, O. Zaleski, O. von Estorff, Evaluation of hypersingular and nearly singular integrals in the isogeometric boundary element method for acoustics, *Computer Methods in Applied Mechanics and Engineering* 325 (2017) 488 – 504.
- 565 [32] Y. Bai, C. Dong, Z. Liu, Effective elastic properties and stress states of doubly periodic array of inclusions with complex shapes by isogeometric boundary element method, *Composite Structures* 128 (2015) 54 – 69.
- [33] R. Simpson, Z. Liu, Acceleration of isogeometric boundary element analysis through a black-box fast multipole method, *Engineering Analysis with Boundary Elements* 66 (2016) 168–182.
- 570 [34] X. Peng, E. Atroshchenko, P., S. Bordas, Isogeometric boundary element methods for three dimensional static fracture and fatigue crack growth, *Computer Methods in Applied Mechanics and Engineering* 316 (2017) 151 – 185. Special Issue on Isogeometric Analysis: Progress and Challenges.
- 575 [35] R. Simpson, Z. Liu, R. Vázquez, J. Evans, An isogeometric boundary

element method for electromagnetic scattering with compatible b-spline discretizations, *Journal of Computational Physics* 362 (2018) 264 – 289.

- [36] J. Dölz, S. Kurz, S. Schöps, F. Wolf, Isogeometric boundary elements in
580 electromagnetism: Rigorous analysis, fast methods, and examples, arXiv
preprint arXiv:1807.03097 (2018).
- [37] K. V. Kostas, A. I. Ginnis, C. G. Politis, P. D. Kaklis, Ship-hull shape
optimization with a T-spline based BEM–isogeometric solver, *Computer
Methods in Applied Mechanics and Engineering* 284 (2015) 611 – 622.
- 585 [38] E. Gillebaart, R. D. Breuker, Low-fidelity 2D isogeometric aeroelastic anal-
ysis and optimization method with application to a morphing airfoil, *Com-
puter Methods in Applied Mechanics and Engineering* 305 (2016) 512 –
536.
- [39] M. Yoon, S. Cho, Isogeometric shape design sensitivity analysis of elasticity
590 problems using boundary integral equations, *Engineering Analysis with
Boundary Elements* 66 (2016) 119 – 128.
- [40] H. Lian, P. Kerfriden, S. Bordas, Shape optimization directly from CAD:
An isogeometric boundary element approach using T-splines, *Computer
Methods in Applied Mechanics and Engineering* 317 (2017) 1 – 41.
- 595 [41] R. Simpson, M. Scott, M. Taus, D. Thomas, H. Lian, Acoustic isogeometric
boundary element analysis, *Computer Methods in Applied Mechanics and
Engineering* 269 (2014) 265–290.
- [42] B. Marussig, J. Zechner, G. Beer, T.-P. Fries, Fast isogeometric bound-
ary element method based on independent field approximation, *Computer
600 Methods in Applied Mechanics and Engineering* 284 (2015) 458 – 488. Iso-
geometric Analysis Special Issue.
- [43] C. A. Brebbia, J. Domínguez, Boundary element methods for potential
problems, *Applied Mathematical Modelling* 1 (1977) 372 – 378.

- [44] J. M. Xu, C. A. Brebbia, Optimum Positions for the Nodes in Discontinuous
605 Boundary Elements, Springer Berlin Heidelberg, Berlin, Heidelberg, 1986,
pp. 751–767.
- [45] P. Parreira, On the accuracy of continuous and discontinuous boundary
elements, *Engineering Analysis* 5 (1988) 205 – 211.
- [46] Y. J. Wang, D. J. Benson, Multi-patch nonsingular isogeometric boundary
610 element analysis in 3D, *Computer Methods in Applied Mechanics and
Engineering* 293 (2015) 71–91.
- [47] E. M. E. Zayed, Hearing the shape of a compact riemannian manifold with
a finite number of piecewise impedance boundary conditions, *International
Journal of Mathematics & Mathematical Sciences* 20 (2007) 397–402.
- 615 [48] J. Guo, G. Yan, M. Cai, Multilayered scattering problem with generalized
impedance boundary condition on the core, *Journal of Applied Mathemat-
ics* 2015 (2015).
- [49] E. Perrey-Debain, J. Trevelyan, P. Bettess, On wave boundary elements
for radiation and scattering problems with piecewise constant impedance,
620 *IEEE Transactions on Antennas and Propagation* 53 (2005) 876–879.
- [50] O. Laghrouche, P. Bettess, E. Perrey-Debain, J. Trevelyan, Wave interpo-
lation finite elements for Helmholtz problems with jumps in the wave speed,
Computer Methods in Applied Mechanics and Engineering 194 (2005) 367
– 381.
- 625 [51] L. Piegl, W. Tiller, *The NURBS Book*, Princeton University Press, 1997.
- [52] D. F. Rogers, *An introduction to NURBS: with historical perspective*, El-
sevier, 2001.
- [53] M. G. Cox, The numerical evaluation of B-splines, *IMA Journal of Applied
Mathematics* 10 (1972) 134–149.

- 630 [54] C. D. Boor, On calculating with B-splines, *Journal of Approximation Theory* 6 (1972) 50–62.
- [55] P. Morse, K. Ingard, *Theoretical Acoustics*, Princeton University Press, 1968.
- [56] S. Marburg, H. J. Hardtke, A study on the acoustic boundary admittance. Determination, results and consequences, *Engineering Analysis with Boundary Elements* 23 (1999) 737–744.
- 635 [57] Y. Liu, T. J. Rudolphi, Some identities for fundamental solutions and their applications to weakly-singular boundary element formulations, *Engineering Analysis with Boundary Elements* 8 (1991) 301–311.
- 640 [58] A. H. Stroud, D. Secrest, *Gaussian quadrature formulas*, Prentice-Hall, 1966.
- [59] J. C. F. Telles, A self-adaptive coordinate transformation for efficient numerical evaluation of general boundary element integrals, *International Journal for Numerical Methods in Engineering* 4 (1987) 959–973.
- 645 [60] H. A. Schenck, Improved integral formulation for acoustic radiation problems, *The Journal of the Acoustical Society of America* 44 (1968) 41–58.
- [61] A. J. Burton, G. F. Miller, The application of integral equation methods to the numerical solution of some exterior boundary-value problems, *Proceedings of the Royal Society of London A: Mathematical, Physical and Engineering Sciences* 323 (1971) 201–210.
- 650 [62] T. Greville, Numerical procedures for interpolation by spline functions, *Journal of the Society for Industrial and Applied Mathematics Series B Numerical Analysis* 24 (1964) 118–173.
- [63] R. Johnson, Higher order B-spline collocation at the Greville abscissae, *Applied Numerical Mathematics* 52 (2005) 63–75.
- 655

[64] S. Marburg, S. Schneider, Influence of element types on numeric error for acoustic boundary elements, *Journal of Computational Acoustics* 11 (2003) 363–386.

[65] J. Zhu, On the Simulation of the Interior Noise of a Light Bus, Ph.D. thesis, 660 Jiangu University, 2005.